

Spectrum of Short-Period Core Phases in Relation to the Attenuation in the Mantle¹

HIROO KANAMORI²

Seismological Laboratory, California Institute of Technology, Pasadena

Spectral analysis is made of the records of the short-period reflected core phases from array stations at Tonto Forest, Arizona. Three earthquakes having $\Delta = 32.5^\circ, 49.0^\circ,$ and 62.8° are studied. Spectral ratios of *ScS* to *ScP* and *PcS* to *PcP* are calculated in order to estimate the differential effect of attenuation on *P* and *S* waves. The possible maximum value of average Q for shear in the mantle, \bar{Q}_β , is about 324 for the period range 1.5 to 5 sec. Using the value of \bar{Q}_α , average Q for *P* waves, that was previously estimated as 435 through the spectral analysis of *PcP* phase \bar{Q}_β and $\bar{Q}_\alpha/\bar{Q}_\beta$ can be estimated at 230 and 1.90, respectively.

Introduction. The attenuation of elastic waves within the mantle has been studied by means of a variety of methods. To relate the observed attenuation to its physical mechanism, it is necessary to determine the distribution of Q , the dimensionless quality factor, with depth, the frequency dependence of Q and the relation between the Q_α, Q for *P* waves, and Q_β, Q for *S* waves.

In this paper the attenuation of short-period ($T = 1.5 \sim 5$ sec) body waves is determined through the spectral analysis of core phases such as *PcP, PcS, ScP,* and *ScS*. Three components seismograms recorded by the Johnson-Matheson short-period instruments at the Tonto Forest Seismological Observatory, Arizona, are used for the analysis. For the period September 1963 to August 1964 three pairs of *ScS* and *ScP* phases and one pair of *PcP* and *PcS* phases were clearly recorded. Table 1 lists the earthquakes, phases, and components used for the analysis. Figure 1 shows the E-W and N-S components of *ScS* and Z components of *ScP* phase of January 26, 1964, earthquake. The phase identifications were mainly based on the arrival time. Whenever available, the arrival times of the corresponding phases at other stations at Blue Mountain, Cumberland Plateau, Uinta Basin, and Wichita Mountains were referred to for confirmation.

Using the spectral ratio of either *ScS* to *ScP* or *PcS* to *PcP* and introducing several reasonable assumptions, we can determine the differential effect of attenuation on *P* and *S* waves from which the possible range of Q_β can be determined.

Analysis. The ray paths of *ScS* and *ScP* phases are schematically illustrated in Figure 2. We will write the frequency spectrum of *ScS* and *ScP* phases at *B* as $ScS(f)$ and $ScP(f)$, respectively.

Then

$$ScS(f) = kI(f)S(f) \cdot \exp \left\{ -\pi f \int_{C_s} \frac{ds}{Q_\beta V_\beta} \right\} \quad (1)$$

$$ScP(f) = k'I(f)S'(f) \cdot \exp \left\{ -\pi f \int_{C_p} \frac{ds}{Q_\alpha V_\alpha} \right\} \quad (2)$$

where

- $I(f)$, instrument response.
- $S(f)$, *S*-wave spectrum at *P*.
- $S'(f)$, *S*-wave spectrum at *P'*.
- C_s , ray path $P \rightarrow B$.
- C_p , ray path $P' \rightarrow B$.
- V_α , *P*-wave velocity.
- V_β , *S*-wave velocity.

k represents the amplitude diminution of *ScS* phase due to various causes, such as the reflection at the core boundary and the geometrical spreading of the ray; k' is the corresponding quantity for *ScP* phase. The integrations are

¹ Contribution 1418, Division of Geological Sciences, California Institute of Technology.

² On leave from Geophysical Institute, Tokyo University.

TABLE 1. List of Earthquakes

Earthquake Number	Date	Origin Time GCT h m s	Latitude	Longitude	Focal Depth, km	Magnitude, C.G.S.	Δ to TFO, deg	Azimuth, deg	Region	Phase	Component
1	Nov. 3, 1963	03 10 12.7	3.5°S	77.8°W	33	6.0	49.0	133	Peru-Ecuador border	ScS ScP	N Z
2	Jan. 26, 1964	09 09 33.9	16.3°S	71.7°W	116	6.1	62.8	137	Southern Peru	ScS ScP	E, N Z
3	July 30, 1964	05 16 03.3	11.1°N	86.2°W	42	5.7	32.5	125	Near west coast of Costa Rica	ScS ScP PcP PcS	E two Z E, N

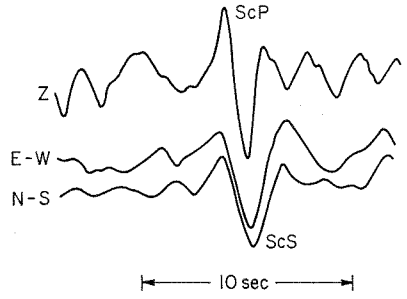


Fig. 1. Short-period seismograms recorded at Tonto Forest, Arizona, showing Z component of ScP phase and E-W and N-S components of ScS phase.

taken along C_s and C_P in (1) and (2), respectively. In the above, it is implicitly assumed that no spectral distortion is caused by the core boundary and the crustal layering. It has been inferred that the core boundary is well defined even for 1-sec period waves [Kanamori, 1967]. For the period range studied here, it is probably reasonable to regard it as a sharp boundary. The effect of the crustal layering can be estimated by Haskell's method [Haskell, 1962]. As will be discussed later, the crustal effect can be ignored in the present analysis.

We will further assume that

1. $S(f) = S'(f)$.
2. $Q_\alpha = \eta Q_\beta$ (η , constant).
- 3.

$$\int_{C_P} \frac{ds}{Q_\alpha V_\alpha} = \frac{1}{1.82\eta} \int_{C_S} \frac{ds}{Q_\beta V_\beta}$$

Assumption 1 is reasonable for two reasons. First, the difference of the take-off angle of

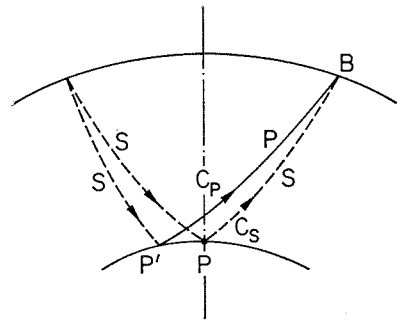


Fig. 2. Schematic illustration of ray paths of ScS and ScP phases.

ScP and ScS at the source is smaller than 7° even for the epicentral distance as large as 60°. Second, since the attenuation in the lower mantle is probably very small, the slight difference between the paths $S \rightarrow P'$ and $S \rightarrow P$ does not greatly change the spectrum of S waves. In assumption 3, the replacement of the path is made for the same reasons, and the mean ratio 1.82 of the P-wave velocity to S-wave velocity within the mantle is introduced.

Dividing equation 1 by equation 2 and taking the logarithm of the absolute value, we have

$$\log \left| \frac{ScS(f)}{ScP(f)} \right| = \log \left(\frac{k}{k'} \right) - \pi \frac{T_\beta(\Delta) f}{\bar{Q}_d(\Delta)} \log e \quad (3)$$

where

$$\bar{Q}_d(\Delta) = \bar{Q}_\beta(\Delta) / (1 - 1/(1.82\eta)) \quad (4)$$

$$\bar{Q}_\beta(\Delta) = T_\beta(\Delta) / \int_{C_s} \frac{ds}{Q_\beta V_\beta}$$

Δ is the epicentral distance, and $T_\beta(\Delta)$ is the travel time of the S wave from P to B and is equal to one-half of the travel time of ScS. $\bar{Q}_\beta(\Delta)$ is the average Q_β along the path C_s . The average Q_β usually defined corresponds to $\bar{Q}_\beta(0)$. The dependence of the ratio $\bar{Q}_\beta(\Delta)/\bar{Q}_\beta(0)$ on Δ is slight. $\bar{Q}_\beta(\Delta)/\bar{Q}_\beta(0)$ for CIT11 velocity model [Anderson and Toksöz, 1963] and MMS' Q_β model, which represents a minor modification of the model given by Anderson et al. [1965], was calculated and tabulated in Table 2. Dependence of $\bar{Q}_\beta(\Delta)/\bar{Q}_\beta(0)$ on the distance will be about the same for other Q models in which attenuation is less in the lower mantle than in the upper mantle.

Using (3) we can determine \bar{Q}_d from the slope of logarithmic plot of the spectral ratio against

TABLE 2. Dependence of $\bar{Q}_\beta(\Delta)$ on Δ

Δ , deg	$\bar{Q}_\beta(\Delta)/\bar{Q}_\beta(0)$
0	1.00
10	1.00
20	1.02
30	1.04
40	1.07
50	1.11
60	1.16
70	1.21
80	1.26

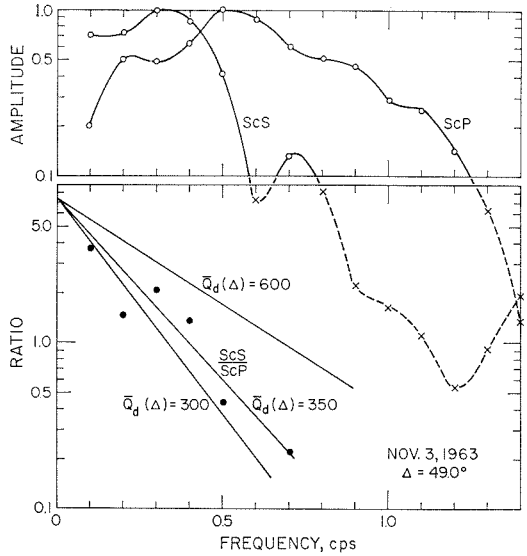


Fig. 3. Amplitude spectrums of ScS and ScP phases for earthquake of November 3, 1963. Dots are the spectral ratios of ScS/ScP.

frequency. Since there are many uncertainties in the absolute amplitude originating from the reflection at the core boundary, local crustal structure, and the instrument magnification, the absolute amplitude ratio k/k' was not used, and only the relative spectral ratio was used.

The spectral analysis of the records was made in the following manner. The time record having $2T_m$ duration was first taken using the time window

$$w(t) = 0.54 + 0.46 \cos \frac{\pi t}{T_m} \quad |t| \leq T_m \quad (5)$$

$$= 0 \quad |t| > T_m$$

$w(t)$ was centered at the arrival time of the main pulse. Then it was digitized at every 0.2 sec. Two values for T_m , 5 and 10 sec, were tried. In case of $T_m = 10$ sec the spectrum was slightly jagged compared with that for $T_m = 5$ sec, but the general trend was about the same.

In Figures 3, 4, and 5, the normalized spectrums for $T_m = 5$ sec are shown. When two traces were available for one component, the average spectrum was used. The shift of the ScP spectrum on the frequency scale with respect to ScS is clearly observed for all cases. For the calculation of the spectral ratio, harmonics whose amplitude is less than 10% of the

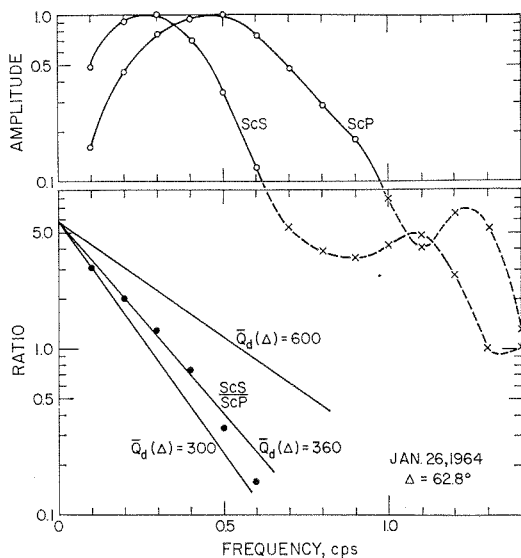


Fig. 4. Amplitude spectra of *ScS* and *ScP* phases for earthquake of January 26, 1964. Dots are the spectral ratios of *ScS/ScP*.

amplitude of maximum harmonic were not used. The ratio thus calculated is plotted by dots. The linear decrease with increasing frequency is clearly seen, as expected. Straight lines are fitted to determine the slope of the spectral ratio.

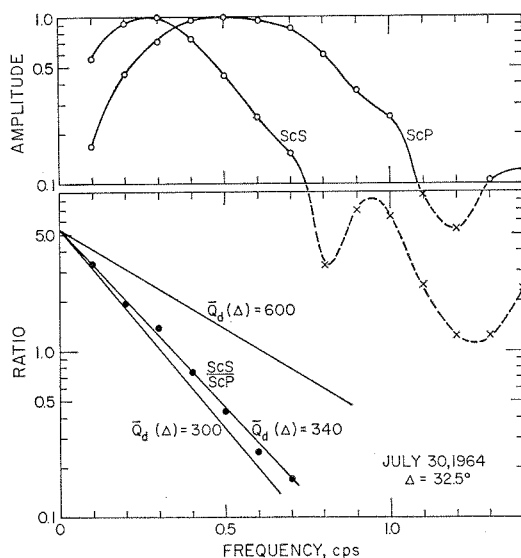


Fig. 5. Amplitude spectra of *ScS* and *ScP* phases for earthquake of July 30, 1964. Dots are the spectral ratios of *ScS/ScP*.

TABLE 3. Summary of Results

Earthquake Number	Δ , deg	Phase	$\bar{Q}_d(\Delta)$	$\bar{Q}_d(0)$
1	49.0	<i>ScS-ScP</i>	350	318
2	62.8	<i>ScS-ScP</i>	360	313
3	32.5	<i>ScS-ScP</i>	340	325
		<i>PcP-PcS</i>	350	340
			Average	324

Two lines corresponding to $\bar{Q}_d(\Delta) = 300$ and $\bar{Q}_d(\Delta) = 600$ are drawn in the figure as references. The results together with the values corrected for the distance based on Table 2 are summarized in Table 3.

The same method applies to the *PcP* and *PcS* pair. The result is given in Figure 6 and Table 3.

The values of $\bar{Q}_d(0)$ determined from earthquakes having different distances and different phases are in fairly good agreement. The average value is 324.

Discussion and conclusion. In order to estimate the crustal effect, which has so far been ignored, a crustal model as given by Table 4 was taken, and the transfer functions were calculated by the Haskell's method. As the angle of incidence of the up-going wave is about

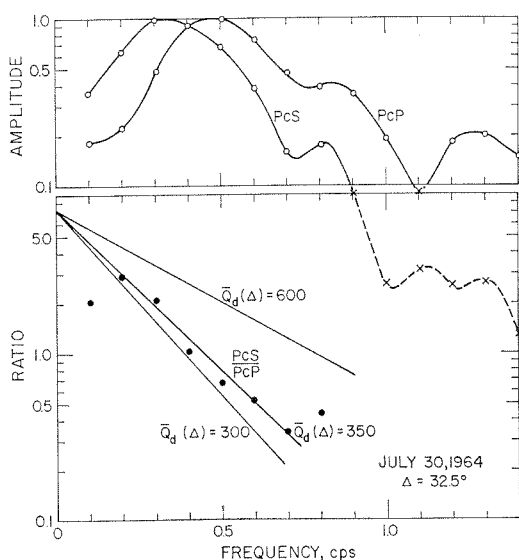


Fig. 6. Amplitude spectra of *PcS* and *PcP* phases for earthquake of July 30, 1964. Dots are the spectral ratios of *PcS/PcP*.

TABLE 4. Crustal Model Used in the Computations of Transfer Functions

	Thickness, km	P-Wave Velocity, km/sec	S-Wave Velocity, km/sec	Density, g/cm ³
1st layer	11.0	6.10	3.50	2.70
2nd layer	9.0	6.40	3.68	2.90
3rd layer	18.0	6.70	3.94	2.90
Half-space		8.15	4.75	3.30

10° ~ 20° at the base of the crust for the epicentral distance range concerned here, four cases are considered: SV-wave incident at the base of the crust with the angle $i_s = 10^\circ$ and 20° , and P-wave incident with the angle $i_p = 10^\circ$ and 20° . The results are given by solid curves in Figure 7. $|U_s|$ is the amplitude spectrum of the horizontal component of the surface displacement for the impulsive SV input at the base of the crust. $|W_p|$ is the vertical component of the surface displacement for P-wave input. The spectrums are rather jagged, varying from 2 to 3. In the present spectral analysis, however, time record of finite length was considered using the time window $w(t)$ given by (5). Let $H(f)$ represent the crustal transfer functions. The effective crustal transfer function $G(f)$ corresponding to the time record cut out by $w(t)$ centered at time t_1 can be written approximately as

$$G(f) = e^{-2\pi i f t_1} \int_{-\infty}^{+\infty} H(f') \mathfrak{W}(f' - f) \cdot e^{2\pi i f' t_1} df' \quad (6)$$

where $\mathfrak{W}(f)$ is the Fourier transform of $w(t)$. The amplitude of $G(f)$ thus calculated for each case considered above is shown by the dotted curves in Figure 7. As expected from (6), the spectrum is smoothed and becomes essentially flat over the frequency range now considered. The crustal effect can, therefore, be ignored.

The value of \bar{Q}_d (for brevity, $\bar{Q}_d(0)$, $\bar{Q}_\beta(0)$, and $\bar{Q}_\alpha(0)$ are denoted by \bar{Q}_d , \bar{Q}_β , and \bar{Q}_α in the following), estimated at 324, can be reduced to \bar{Q}_β if we assume the value of η . Using (4), several solutions are given in Table 5. It is obvious that \bar{Q}_d gives possible maximum value of \bar{Q}_β . The value of η depends on the physical mechanism of attenuation, and, though there is no widely accepted theory as to what value η should take,

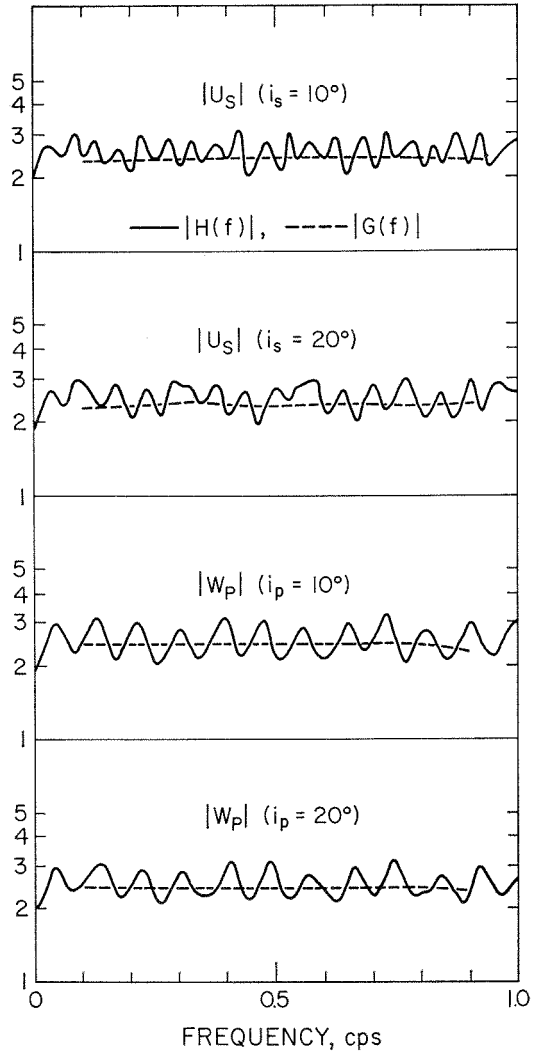


Fig. 7. Normalized crustal transfer functions for SV incidence (U_s) and P incidence (W_p). Solid curves are for time record of infinite length. Dotted curves are for time record of 10-sec length.

TABLE 5. Estimate of \bar{Q}_β for Various η

η	\bar{Q}_β	\bar{Q}_α
1	146	146
1.90*	230	435
2	235	470
3	264	792
5	288	1440
∞	324	∞

*Solution with $\bar{Q}_d = 324$ and $\bar{Q}_\alpha = 435$.

η of $1 \sim 3$ seems most probable. In this case the upper and lower bounds of \bar{Q}_β are 150 and 260, respectively.

If we combine the value of \bar{Q}_α that was previously determined through the spectral analysis of short-period *PcP* phase [Kanamori, 1967], we can determine η and \bar{Q}_β separately. It was shown that MMS' Q distribution is a good approximation for Q_α around the period of $1 \sim 2$ sec. The average Q of MMS' model is about 435. Using this value for \bar{Q}_α and the relation of (4) together with $\bar{Q}_\alpha = \eta \bar{Q}_\beta$, we obtain $\bar{Q}_\alpha = 435$, $\bar{Q}_\beta = 230$, and $\eta = 1.90$, as shown in Table 5.

The value of \bar{Q}_β obtained here appears to be definitely small compared with the previous estimates by Press [1956] ($\bar{Q}_\beta = 500$, $T = 11$ sec), Anderson and Kovach [1964] ($\bar{Q}_\beta = 500$, $T = 25$ sec), and Kovach and Anderson [1964] ($\bar{Q}_\beta = 600$, $T = 15 \sim 75$ sec). Even allowing for the experimental uncertainties, this difference still seems significant. These results may indicate that \bar{Q}_β decreases with increasing frequency. \bar{Q}_β around 2 sec may be small by a factor of 2 compared with \bar{Q}_β around $25 \sim 50$ sec. However, the short-period records are often disturbed by various reverberations of unknown origin. Since the effect of these reverberations on the individual spectrum is difficult to evaluate, it is necessary to increase the number of data before we can definitely establish the frequency dependence of Q .

Acknowledgment. I am grateful to Drs. Don L. Anderson, C. B. Archambeau, J. N. Brune, and L. R. Johnson for various suggestions that are included in the final manuscript.

Research was partially sponsored by the Air Force Office of Scientific Research, Office of Aerospace Research, United States Air Force, under AFOSR contract AF-49(638)-1337.

REFERENCES

- Anderson, Don L., Ari Ben-Menahem, and C. B. Archambeau, Attenuation of seismic energy in the upper mantle, *J. Geophys. Res.*, **70**, 1441-1448, 1965.
- Anderson, D. L., and R. L. Kovach, Attenuation in the mantle and rigidity of the core from multiply reflected core phases, *Proc. Natl. Acad. Sci. U. S. A.*, **51**, 168-172, 1964.
- Anderson, Don L., and M. Nafi Toksöz, Surface waves on a spherical earth, 1, Upper mantle structure from Love waves, *J. Geophys. Res.*, **68**, 3483-3500, 1963.
- Haskell, Norman A., Crustal reflection of *P* and *SV* waves, *J. Geophys. Res.*, **67**, 4751-4767, 1962.
- Kanamori, Hiroo, Spectrum of *P* and *PcP* in relation to the mantle-core boundary and attenuation in the mantle, *J. Geophys. Res.*, **72**, 559-571, 1967.
- Kovach, R. L., and D. L. Anderson, Attenuation of shear waves in the upper and lower mantle, *Bull. Seismol. Soc. Am.*, **54**, 1855-1864, 1964.
- Press, F., Rigidity of the earth's core, *Science*, **124**, 1204, 1956.

(Received September 22, 1966.)